10-31-02 11:43 RC

REPORT DOCUMENTATION PAGE

AFRL-SR-AR-TR-02-

0371

1. AGENCY USE ONLY *(Leave blank)*	2. REPORT DATE	3. REPORT TYPE AND DATES COVERED
	28 October 2002	Final Report, 30 Sept 2001 -29 September 2002

6. TITLE AND SUBTITLE
Crested Tunnel Barriers for Fast, High Density, Nonvolatile Memory Devices

7. FUNDING NUMBERS
F49620~~-01-0059~~
01-C0059

8. AUTHORS
David Hamblen, Joseph Cosgrove

9. PERFORMING ORGANIZATION NAME(S) AND ADDRESS(ES)
Advanced Fuel Research, Inc.
87 Church Street
East Hartford, CT 06108-3728

State Univ. of New York
Stony Brook, NY 11794-3800

10. PERFORMING ORGANIZATION REPORT NUMBER
526052

11. SPONSORING/MONITORING AGENCY NAME(S) AND ADDRESS(ES)
Department of Defense
US AF Office of Scientific Research
801N. Randolph Street, Rm 732
Arlington, VA 22203

10. SPONSORING/MONITORING AGENCY REPORT NUMBER

11. SUPPLEMENTARY NOTES

12a. DISTRIBUTION/AVAILABILITY STATEMENT
Approved for public release; distribution unlimited

12b. DISTRIBUTION CODE

13. ABSTRACT *(Maximum 200 words)*

Report developed under STTR Contract for Topic AF01-T003. Crested multi-layer tunnel barriers have been proposed, which offer a revolutionary solution to overcome density to speed trade-offs characteristic of present data storage technologies. Practical implementation of the proposed technology will involve use of thin film materials that are readily manufacturable and CMOS-compatible. A critical need exists for experimental verification of the theoretical predictions regarding these advanced structures. In addition, challenges lay ahead in developing a suitable deposition technology for fabrication of the ultra-thin graded or multilayered structures involved. Advanced Fuel Research, Inc., and the State University of New York at Stony Brook will develop a technology for fabrication of crested tunnel barrier devices based on promising thin film material combinations. Phase I research demonstrated tunneling in thin film barrier structures in good agreement with theoretical predictions. Phase II will continue development of tunneling theory and optimize the process for fabricating layered tunnel barrier structures.

14. SUBJECT TERMS
STTR Report, Thin Film, Silicon, Crested Barrier, Tunneling

15. NUMBER OF PAGES
24

16. PRICE CODE

17. SECURITY CLASSIFICATION OF REPORT	18. SECURITY CLASSIFICATION OF THIS PAGE	19. SECURITY CLASSIFICATION OF ABSTRACT	20. LIMITATION OF ABSTRACT
Unclassified	**Unclassified**	**Unclassified**	**Unclassified**

Advanced Fuel Research, Inc., 87 Church Street, East Hartford, CT 06108 USA

PHASE I
FINAL REPORT

"Crested Tunnel Barriers for Fast, High Density, Nonvolatile Memory Devices"

Air Force Contract No: F49620-01-0059

Final Report – 0001AD
Report Period: 30 September, 2001 – 29 September, 2002
Contract Period: 30 September, 2001 – 29 September, 2002

Prepared For:
Department of the Air Force
Air Force Office of Scientific Research

Prepared By:

Dr. David G. Hamblen
Joseph Cogrove
Advanced Fuel Research, Inc.
87 Church Street
East Hartford, CT 06108

Konstantin K. Likharev
Elena Cimpoiasu
Sergey Tolpygo
Xueqing Liu
Nikita Simonian
Ted Feldman
State University of New York at Stony Brook
Stony Brook, NY 11794-3800

AFR Project No.: 526052

October 28, 2002

UNCLASSIFIED

Table of Contents

a. The Problem

Semiconductor memories are one of the most vital components of the electronics world. The mainstream digital technology relies on three centerpiece memory types [1,2]: 1) static random access memories (SRAM), 2) dynamic random access memories (DRAM), floating gate, and 3) non-volatile (e.g., "flash") memories. The coexistence of these memories in many electronic devices indicates that each has limitations. SRAM is faster than its counterparts (cycle times in single nanoseconds), but takes up more chip real estate and much more power. DRAM is simple, relatively fast (cycle times in tens ns), and may be denser than SRAM (1 Gb chips have been demonstrated), but is inherently very difficult to scale because the DRAM cell capacitance should be large enough to charge the output line all the way down to the sense amplifier, regardless of the minimum feature size.

In contrast, floating gate memories may be scaled to very high densities (beyond 10^{11} cells per cm^{-2}), in addition to being nonvolatile. However, they require much longer time (in microseconds) for writing and erasing the data. This drawback restricts the application of floating gate memories to niches where data is written in large blocks and does not allow them to compete for the much broader market of random access memories for which fast (few-nanosecond) write/erase operations and high cell endurance are necessary.

Crested multi-layer tunnel barriers have been proposed [3-5], which offer a revolutionary solution to overcome density to speed trade-offs characteristic of present data storage technologies. Although published articles [3-5] suggest fabrication of these crested barriers based on wide-bandgap semiconductors such as $Al_xGa_{1-x}N$, the authors believe that practical implementation of the proposed technology will involve use of thin film materials which are readily manufacturable and CMOS-compatible. Most recently, crested barriers based on AlO_x/Al_2O_3 have been identified as very promising. There is, however, a critical need for experimental verification of the theoretical predictions regarding these advanced structures. In addition, challenges lay ahead in developing a suitable deposition technology for fabrication of the ultra-thin graded or multilayered structures involved.

b. Phase I Technical Objectives

The overall goal of this Phase I STTR project was for Advanced Fuel Research, Inc. (AFR) and the State University of New York (Stony Brook) at Stony Brook to demonstrate the feasibility of crested tunnel barrier devices through both experimental and theoretical studies. The Phase I project was to be accomplished in the following three tasks:

Task 1 – Tunnel Barrier Fabrication (AFR) – To fabricate simple, two-layer crested barrier structures and to measure the electronic (tunneling) and structural characteristics of the fabricated devices.

Task 2 – Modeling (Stony Brook) – To compare experimental results with theoretical models of tunneling through complex barrier structures.

Task 3 – Manufacturing Studies – To evaluate deposition technologies for fabricating crested tunnel barriers.

c. Phase I Results

The Phase I results are provided below by task. Task 1 describes the experimental facilities and processes at both AFR and Stony Brook employed for fabricating the aluminum oxide tunnel barrier structures. Task 2 presents the results of the electrical characterization of the tunnel barriers along with comparisons to theoretical models. Task 3 describes preliminary deposition studies involving reactive DC sputter deposition.

Task 1 – Tunnel Barrier Fabrication (AFR)

Objective: To fabricate simple, two-layer crested barrier structures and to measure the electronic (tunneling) and structural characteristics of the fabricated devices.

Work Performed: Work performed during this Phase I project concentrated on fabrication and characterization of aluminum oxide barrier layers at both AFR and Stony Brook. AFR focused on aluminum oxide layers deposited primarily by pulsed laser deposition (PLD) and also some initial studies of aluminum oxide deposited by reactive DC magnetron sputtering. Stony Brook concentrated on aluminum oxide layers formed by deposition of aluminum followed by various methods of post oxidation.

Stony Brook – Stony Brook investigated variations of fabricating alumina layers by post oxidation (deposition of pure aluminum layers followed by oxidation) including room temperature thermal oxidation, high temperature thermal oxidation and plasma oxidation. In addition, Stony Brook also explored the effects of rapid thermal annealing on the post oxidized layer properties.

The aluminum oxide barrier structures fabricated for electrical characterization were based on Nb-trilayer ($Nb/Al/AlO_x/Nb$) structures deposited on two inch Si substrates. The typical fabrication sequence is as follows. A 150 nm Nb film is deposited by dc magnetron sputtering in a cryopumped system with a base pressure of 2×10^{-7} Torr. The base electrode is then coated by a similarly sputtered Al layer, 8 nm to 10 nm thick. The Al layer is then oxidized at room temperature in a static dry oxygen atmosphere in the pressure range from 1 to 100 Torr for time intervals ranging from 25 minutes to 40 hours to achieve the desired barrier transparency.

Following the oxidation step, the chamber is again pumped down to base pressure and a 150 nm Nb counter electrode is sputtered. Wafers were patterned by optical lithography with PMMA resist and reactive ion etching in SF_6 plasma. Each 5×5 mm^2 chip had 18 tunnel junctions with sizes ranging from 3×3 μm^2 to 300×300 μm^2. After the junction etch, the PMMA etch mask was used as a mask to lift off a 150 nm SiO_2 dielectric layer insulating the base electrode from the wiring layer (the so-called self aligned lift-off process). Finally, a 300 nm Nb wiring layer was deposited and patterned using lift-off, with wiring configured to enable four-point measurements.

Junction quality was checked first by measuring the low-voltage *I-V* curves at 4.2 K, which demonstrated a sharp superconducting energy gap of niobium at $V_g \approx 2.75$ mV and low subgap leakage. Only the junctions which passed this test were used for high voltage measurements. (The yield of such samples on the wafers discussed below was close to 100%.) These measurements were done on samples immersed directly to liquid helium ($T = 4.2$ K), using the automated setup *Octopux* [6]. This system uses a set of D/A converters to provide sample with a computer controlled dc bias current which is measured from voltage drop across a serially connected 2 kΩ resistor.

In addition to room temperature thermal oxidation, Stony Brook also performed a preliminary investigation of the effect of temperature on the properties of post oxidized alumina layers, studying two effects: 1) high temperature oxidation at 400 °C and 2) rapid thermal annealing of thermal oxide films.

Stony Brook also investigated aluminum oxide barrier layers formed using plasma oxidation in 15 mTorr oxygen atmosphere for 5 min. Fabrication of the overall test structure (substrate, electrodes, barrier layer) is essentially the same, however the alumina barrier is formed by exposing the Al coating to an rf plasma in 15 mtorr of flowing oxygen at room temperature. As with the thermal oxide barriers, a brief investigation of the effects of rapid thermal annealing was also performed.

AFR – Aluminum oxide barrier layers studied investigated at AFR during this Phase I program were primarily deposited by the method of pulsed laser deposition (PLD). In PLD, an intense pulsed laser beam (typically ultraviolet) is focused onto a target, resulting in a highly energetic plasma, the so-called plume, of neutrals and ions which are directed onto a substrate. Energies of arriving atoms can range from less than 1 eV to more than 100 eV, depending on the deposition parameters [7]. The energetic vapor is generally considered advantageous for enhancing layer by layer growth and for producing thin film layers with improved crystallinity, better adhesion and higher density. Another advantage of PLD is that it operates in a "pulsed" mode, which provides an on-off deposition environment, enabling precise control of film thickness. Metal oxide materials such as aluminum oxide can be deposited using ceramic targets (i.e. Al_2O_3) or, in many cases, by using a pure metal target in a background of oxygen – a reactive type deposition.

The PLD system at AFR, shown in Figure 1, employs a quadrupled Continuum Nd:YAG laser (266 nm, ~ 4 ns pulsewidth) with a variable repetition rate from 1 – 10 Hz. The deposition chamber is a six-way stainless steel cross (6-inch i.d.), pumped by a high vacuum turbomolecular pump to an ultimate vacuum of ~ 10^{-7} Torr. Radiative heating of substrates 25 mm x 25 mm in the range of 30-1200 °C is provided by silicon carbide heating elements. The substrate heater, which supports the substrate, is affixed to a linear motion feedthrough. This arrangement allows the target to substrate distance to be varied, which can be used to adjust the deposition rate and film uniformity. Oxygen (ultra-high purity, research grade) flow is controlled by a precision needle valve.

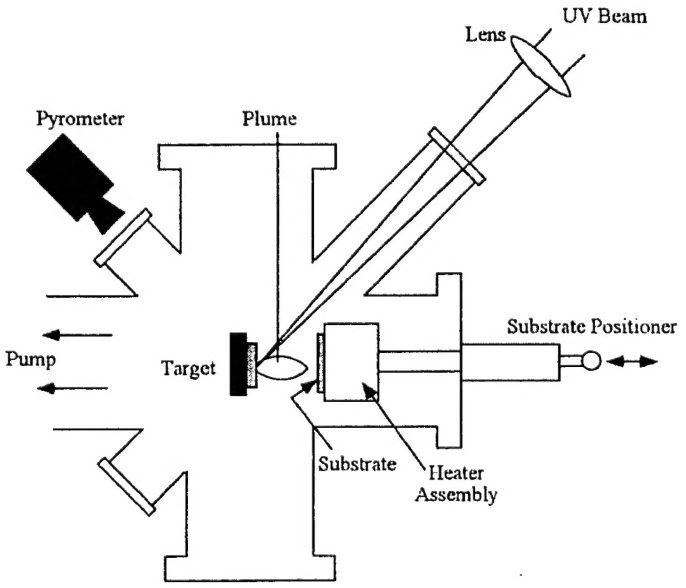

Figure 1. Pulsed laser deposition system employed at AFR for deposition of aluminum oxide thin film barrier layers.

The PLD aluminum oxide thin films studied in this Phase I were deposited from both pure aluminum (99.999 % purity) targets (reactive deposition in a background of ultra-high purity oxygen) and Al_2O_3 (99.99%) targets onto 25 mm x 25 mm square bare silicon and SiO_2-coated silicon substrates (a metal retainer plate limits film coverage to the central 22 mm x 22 mm region of the substrate). Deposition parameters we explored included the oxygen pressure, laser fluence (energy density at the target surface) and substrate temperature. The films were characterized by scanning electron microscopy (SEM), infrared (IR) reflectance spectroscopy, x-ray diffraction (XRD) and Ruthersford backscattering spectroscopy (RBS) as well as electrical measurements (discussed below in Task 2).

We first evaluated films deposited from the pure Al target as it was expected that the film composition could be widely varied from pure aluminum to a sub-oxide (AlO_x) to stoichiometric Al_2O_3 by adjusting the oxygen pressure and/or deposition rate during deposition. We found that films deposited at the base pressure of the chamber (~ 5 x 10^{-7} Torr) were essentially conducting (determined by simple two-point resistance measurements) and visually appeared smooth and silvery as would be expected for a metallic surface. Depositing in 7 x 10^{-6} Torr oxygen increased the film resistance by more than two orders of magnitude, although visually the appearance was similar to the more conductive samples. Raising the oxygen pressure to 5 x 10^{-5} Torr, however, not only increased the film resistance but also altered the film color, suggesting further oxidation of the aluminum layer. Although these results indicated that the aluminum oxide composition is indeed sensitive to the oxygen pressure, we found through SEM analysis that the films were accompanied by an unacceptably high density of particles. Figure 2 presents an SEM image of a ~ 50 nm thick aluminum film deposited on silicon at room temperature, base pressure and a laser fluence of ~ 2.5 J/cm^2, revealing many spherical particles ranging from 1 – 10 μm in diameter. The cause of the particle deposition is probably due to "splashing" from the target during ablation [1]. We found that varying the laser fluence (0.6 – 4 J/cm^2) had little effect on the particle deposition. Note that, aside from the particle deposition, the Al films were smooth and featureless within the resolution of our SEM (~ 50 nm).

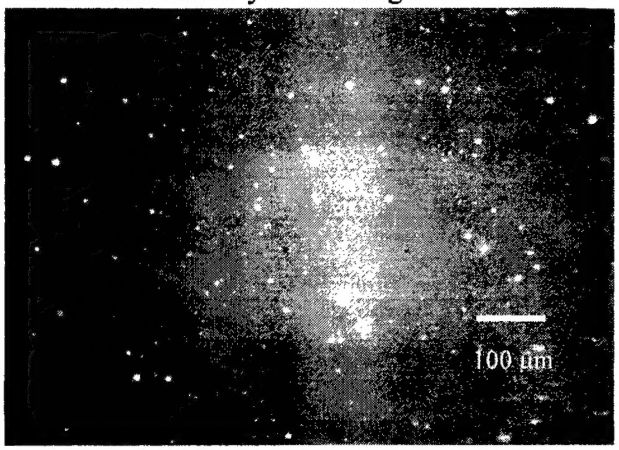

Figure 2. SEM image of a pulsed laser deposited Al film, revealing a high density of particles ejected from the Al target.

In contrast, the particle density on films deposited from the Al_2O_3 target was found to be significantly lower, making these films much more suitable for subsequent device testing. In addition, films as thick as 250 nm displayed a smooth morphology at the SEM resolution limit. Our efforts next focused on establishing the deposition rates of Al_2O_3 films formed under varying deposition conditions, as well as the film optical properties and composition. IR reflectance measurements, obtained at MKS Instruments, were employed to characterize the refractive index (n) and film thickness of relatively thick (250 – 500 nm) films grown on

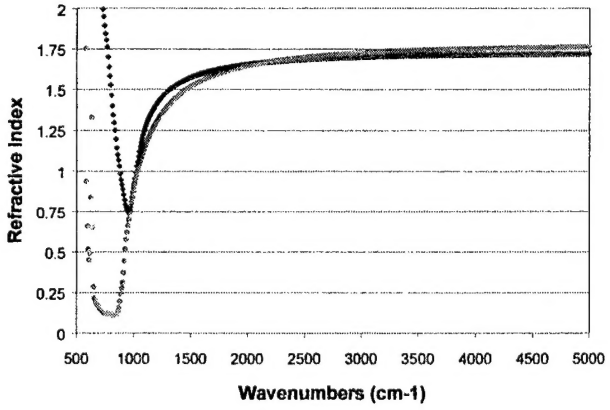

Figure 3. Comparison of refractive index measured for a PLD Al_2O_3 film (blue) to sapphire (red).

Si. Figure 3 compares the refractive index, as a function of wavenumber, of an Al_2O_3 film deposited in 10 mTorr oxygen, a laser fluence of ~ 2.0 J/cm^2 and a substrate temperature of ~ 300 °C, to that of sapphire (single crystal Al_2O_3). In the range 2000 – 5000 cm^{-1} (5 – 2 μm), where the absorption index of Al_2O_3 is negligible, n_{film} (1.65 – 1.72) is quite close to that of $n_{sapphire}$ (1.64 – 1.76). This is an encouraging result, suggesting that the film is highly dense. Note that n_{film} deviates significantly from the sapphire, which is believed to be due to the difference in crystallinity between the amorphous film and the single crystal sapphire sample. XRD measurements performed by H & M Analytical confirmed the amorphous nature of the film.

The IR reflectance measurements also allowed us to determine the deposition rate (which is generally linear for our system), which would be necessary for evaluation of the electrical properties of the very thin barrier structures evaluated in Task 2. Figure 4 depicts a typical reflectance spectrum for an aluminum oxide film deposited on silicon at 300 °C in 0.05 mtorr oxygen. Also shown is a predicted spectrum for a 249 nm (± 2 nm) layer of aluminum oxide, which fits the experimental data very well. In general, the deposition rate for films grown at 300 °C at oxygen pressures below 1 mTorr was found to be ~ 0.13 nm/sec.

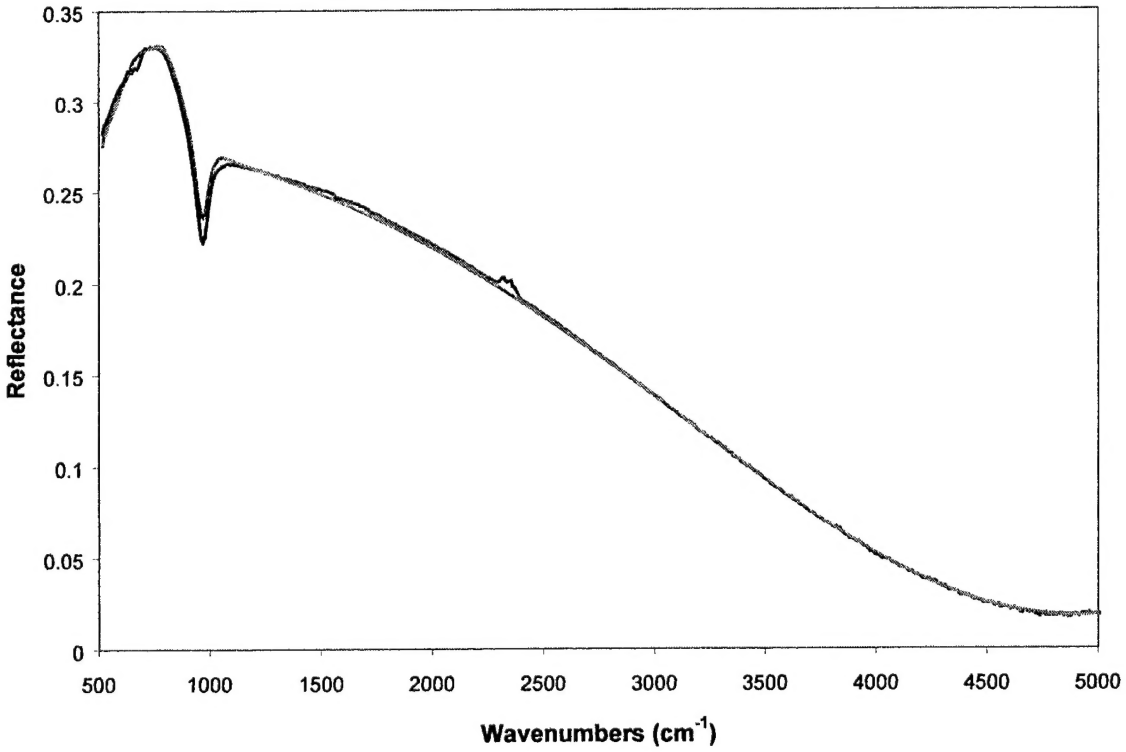

Figure 4. Experimental (blue) and predicted (red) reflectance spectrum for a PLD aluminum oxide film deposited on silicon with the following deposition parameters: substrate temperature = 300 °C, laser fluence = 2.0 J/cm^2, oxygen pressure = 0.05 mTorr, pulse repetition rate = 10 Hz. The sharp dip in reflectance just below 1000 cm^{-1} is an absorption feature due to the aluminum oxide.

RBS measurements (measured at Thin Film Analysis, Inc.) were obtained to investigate the influence of oxygen pressure on the film stoichiometry during deposition. Table 1 compares the Al/O ratio for several relatively thick aluminum oxide films deposited in oxygen background pressures ranging from 0.002 mTorr up to 100 mTorr on low resistivity silicon substrates. For all samples the laser fluence was ~ 2.0 J/cm^2, the repetition rate was 10 Hz and the target to substrate distance was ~ 6 cm. The film thickness indicated for each sample was determined by FTIR reflectance spectrometry.

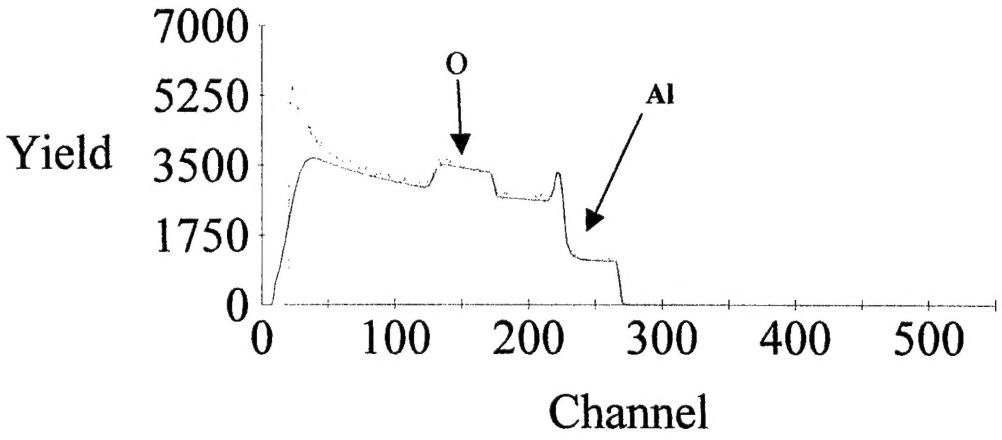

Figure 5. RBS measurement (red) and theoretical model (black) obtained for a PLD aluminum oxide film deposited on silicon at 300 °C in .002 mtorr oxygen. The analysis indicates that this sample is stoichiometric Al_2O_3.

Table 1. Al/O composition measured by RBS for various PLD aluminum oxide films.

Sample	Oxygen Pressure (mtorr)	Substrate Temp. (deg C)	Film Thickness (nm)	Al Fraction	O Fraction	Density (g/cm3)
f020308a	10	500	148	0.4	0.6	3.20
f020308b	10	100	194	0.4	0.6	2.99
f020319a	0.002	300	309	0.4	0.6	3.48
f020319b	0.05	300	303	0.4	0.6	3.68
f020320a	100	300	177	0.34	0.66	1.85
f020320b	0.5	300	232	0.4	0.6	3.52
f020321a	10	300	166	0.4	0.6	3.28

The RBS measurements that indicate that the stoichiometric films are achieved in a broad range of oxygen backgrounds from 0.002 – 10 mTorr, attesting to the strong affinity of Al for O. The RBS technique also provides a measurement of atoms/cm^2, and in combination with the film thickness measurement, the film density can be determined, as shown in Table 1. The samples deposited at 10 mTorr or less are roughly 90 % dense or greater compared to that of bulk alumina oxide (3.97 g/cm^2). With this limited data set we also note a reduction in film density for film deposited at the lowest temperature (100 °C). A dramatic reduction in film density is observed in the sample deposited in 100 mTorr oxygen. This effect may be due to the loss in energy or "thermalization"of the PLD plume, which often occurs at pressures above 10 mTorr[8].

The PLD aluminum oxide barrier structures for electrical characterization were prepared as follows:

1) RCA clean of the p+ silicon substrate ending with removal of the native oxide with dilute HF,
2) Deposition (PLD) of thin aluminum oxide layer directly onto silicon substrate (base electrode),
3) DC magnetron sputter deposition of aluminum contact strips on silicon substrate edges,

4) Vacuum anneal at ~ 450 °C for 30 minutes to form Al/Si ohmic contact,
5) Patterning by photolithography with EPON Su-8 resist and wet chemical etch processing,
6) Sputter deposition of aluminum top contact electrode through shadow mask.

Figure 6 depicts a schematic of the final barrier structure employed for electrical testing of the PLD aluminum oxide. Each sample had 8 – 90 μm x 90μm tunnel junctions. Current-voltage measurements were performed using a computer-controlled Keithley model 230 voltage source in conjunction with a Fluke model 8842A multimeter measuring the voltage drop across a serially connected 10 kΩ resistor.

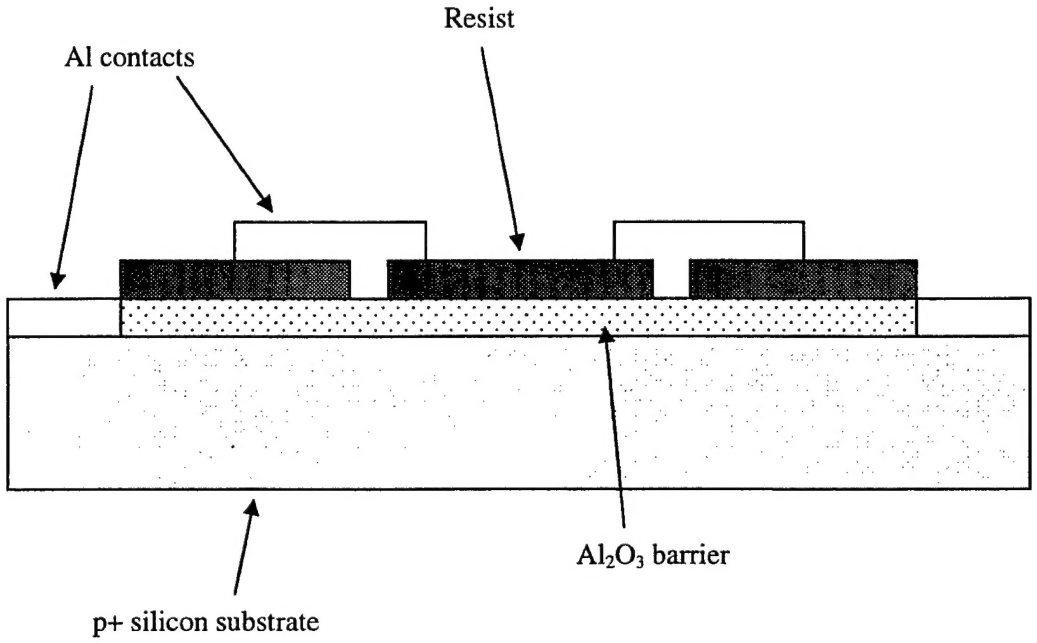

Figure 6. Schematic of thin film barrier structure fabricated for *I-V* measurements at AFR.

Task 2 – Modeling

Objective: To compare experimental results with theoretical models of tunneling through complex barrier structures.

Work Performed:

Post-oxidized Aluminum Oxide Barriers at Stony Brook - During the Phase I work, experimental effort at Stony Brook was focused on aluminum oxides grown on metallic aluminum at various conditions of post-oxidation.[1] Such tunnel barriers serve as the basic components of devices used in low-temperature superconductor electronics (including superconducting quantum computing) and metallic single-electronics; they are also employed in spintronics. However, prior literature data concerning the shape of these barriers was very sketchy, especially in the range of relatively high oxygen exposure, $E \sim 10^5$ Pa-s corresponding to specific zero-field conductances below ~ $10^{10}\ \Omega^{-1}m^{-2}$, i.e. critical currents below ~1 kA/cm^2 in niobium-trilayer Josephson junctions. If we

[1] Stony Brook also explored plasma-grown AlF_3 barriers, which form high-quality, reproducible Josephson junctions. Unfortunately, these barriers have shown rather weak dependence of dc conductivity on applied electric field, and its very substantial temperature dependence. This behavior is indicative of Poole-Frenkel type hopping conductance rather than the direct tunneling necessary for crested barrier applications.

restrict our attention to the most natural option of nearly-room-temperature oxidation in this exposure range, we are aware of only very few publications [9-13] where the average barrier height ϕ_a and physical barrier thickness d had been derived from tunneling data. The additional difficulty is that the authors of the cited works, just as most other authors studying tunnel barrier shape, used the WKB formulas derived by Simmons [14] and Brinkman *et al.* [15] for fitting. As will be shown below, the WKB approximation gives significant errors for barriers so thin.

Room Temperature Thermal Aluminum Oxide Barriers – Table 2 lists fabrication parameters and breakdown voltages for three aluminum oxide barrier samples formed by room temperature thermal oxidation at Stony Brook. These regimes cover essentially the whole range from very thin barriers near the crossover between resonant and direct tunneling (**Cr02**) to practically the thickest barriers which can be grown without additional oxidation means (**Cr12**). Experimental measurements (which were carried out typically at 4.2K to eliminate the thin film electrode resistance effects) showed that this increase of exposure leads to a gradual increase of barrier resistance from ~5×10^{-6} Ω-cm^2 (for **Cr02**) to ~ 2×10^{-4} Ω-cm^2 (for **Cr12**) – see Figure 7, approximately proportional to $E^{1/2}$.

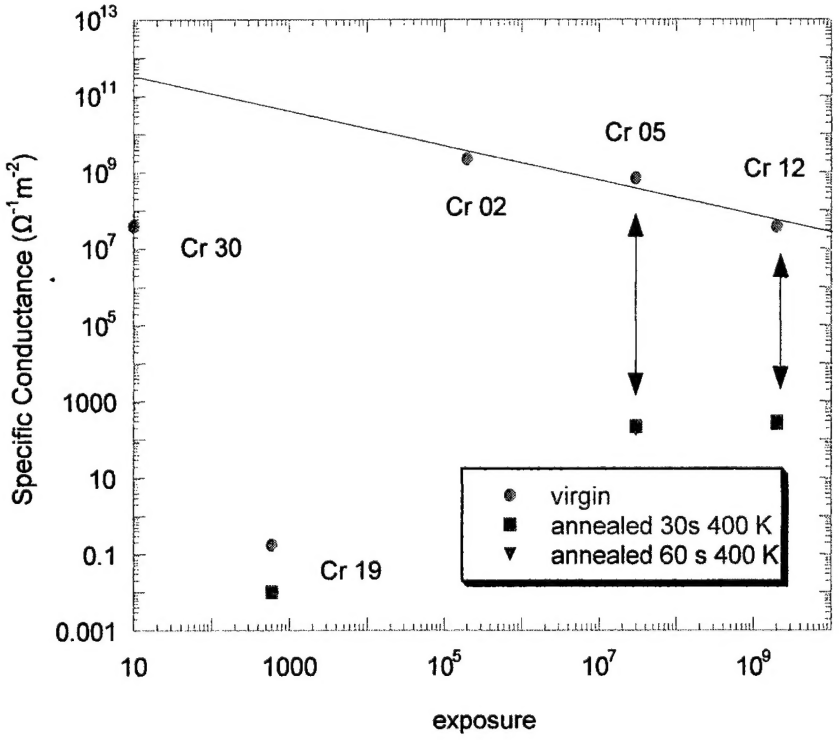

Figure 7. Low-voltage specific conductance G_0 of Nb/Al/AlO_x/Nb junctions with thermally grown and plasma-oxidized tunnel barriers before (red) and after (blue and green) annealing at 400°C, as a function of oxygen exposure E (in Pa-s). The solid line shows the $G_0 \propto E^{1/2}$ trend noted earlier (for exposures $E < 10^6$ Pa-s) by Miller *et al.* [16].

Table 2. Fabrication Parameters and Breakdown Voltages for Thermal Aluminum Oxide Barriers

Wafer #	Oxygen Pressure (Torr)	Oxidation Time	Oxygen Exposure (Pa-s)	Breakdown Voltage (V)
Cr02	2.5	10 minutes	2×10^5	0.80±0.05
Cr05	100	40 minutes	3×10^7	1.03±0.05
Cr12	100	40 hours	2×10^9	1.65±0.12

The junctions exhibited "hard" breakdown at certain voltages V_{break} ranging from 0.8 V for thinner barriers to 1.6 V for thicker barriers – see Table 2. Approximately 0.1V below the breakdown, some irrevocable changes of junction properties ("soft breakdown") might be noticed – see Figure 8. In order to recognize these changes (and exclude these regions from data fitting), the applied current was repeatedly swept back and force about the origin, with gradually increased amplitude. Outside of the soft breakdown region, the *I-V* curves were quite reproducible, both across the chip and across each wafer. Another indication of high quality of the oxide layers is that the breakdown field is very high, 10 MV/cm. This quality is necessary for the successful operation of planned crested barriers [3,17].

In order to avoid the WKB approximation errors, we have also fitted our data with theoretical results calculated using the (virtually) exact numerical transfer-matrix calculation of barrier transparency for each electron energy, and then summing it up (also numerically) for all relevant electron energies. Though this procedure is more time consuming than the WKB calculation, it has been optimized to calculate the whole dc *I-V* curve (in ~10^2 points) in just a few minutes on a modern workstation.

In contrast to the WKB approximation, the exact solution requires Fermi energies E_F of electrode metals; however, the resulting dependence on these parameters is weak. Following the free electron gas estimates [18], we have accepted $E_F = 11.7$ eV for aluminum and $E_F = 5.3$ eV for niobium. In the same spirit, the electron mass in both electrodes was taken to be equal m_0. However, the effective electron mass m inside the barrier affects the results strongly. Fortunately, our calculations have shown that at least within the reasonable range of m (from 0.2 to $1.0m_0$) the results virtually do not depend on m and d if the "effective thickness" $d_{ef} \equiv (m/m_0)^{\alpha}d$ is kept constant. In our parameter range, the scaling coefficient α changes very little, from 0.433 for wafer Cr02 to 0.450 for Cr12. (Note that within the WKB approximation the results are *exactly* independent of m and d if d_{ef}, with $\alpha = 0.50$, is constant.)

Figure 8 shows the experimental data for the nonlinear conductance $G \equiv dI(V)/dV$ for typical samples from all three wafers, and their best theoretical fits using the usual trapezoidal model for the tunnel barrier profile. They show, in particular, that the barrier parameters derived from microscopic theory fitting differ substantially from those from WKB fitting. The comparison of the experimental data and calculation results shows that, on one hand, the theory gives reasonable fits only within a narrow range of barrier parameters, so that the formal fitting error bars for each sample are fairly narrow.

On the other hand, it is clear that the direct electron tunneling, which is the only transport mechanism taken into account in our theory, cannot describe all the observed data features. Leaving alone the superconducting gap structure at low voltages and irrevocable junction changes in the soft breakdown region, two features are especially noticeable:

1) A hysteretic loop at positive voltages (positive potential of the Nb counter-electrode) between ~0.45 and ~0.6 V. (This feature is more pronounced for thinner barriers.)
2) A virtually non-hysteretic excess current at negative voltages, starting from the origin and persisting almost to $V = -1$ Volt.

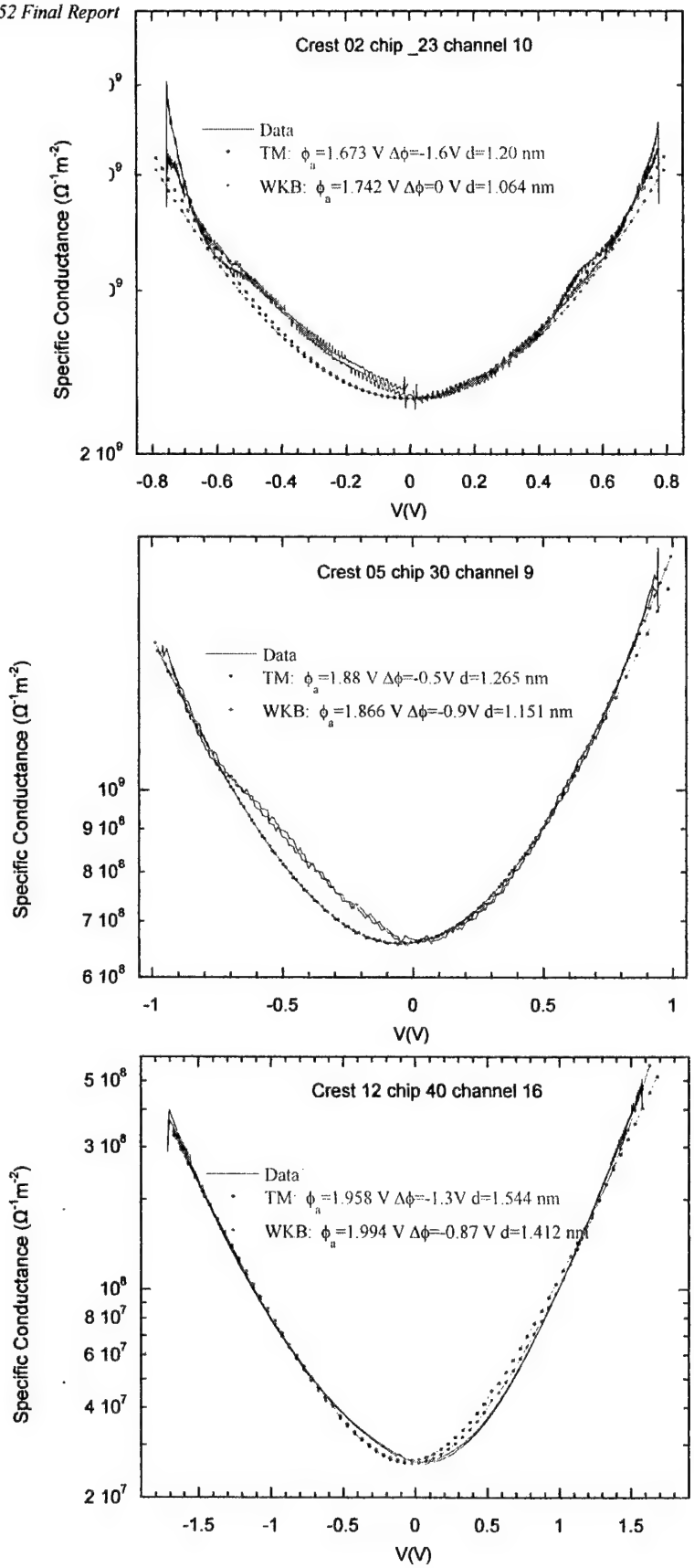

Figure 8. Nonlinear specific conductance of thermally oxidized AlOx barriers as a function of applied voltage, and its best fitting using WKB and microscopic ("TM") theories for trapezoidal barrier model. The listed barrier thickness is for the effective mass $m = 0.5\ m_0$.

The average fitting results are summarized in Table 3 (which also lists the results for other AlO_x barriers, as discussed below).

Table 3. Summary of AlO_x Barrier Fitting Results

Wafer#	G_0 ($\Omega^{-1}\cdot m^2$)	ϕ_a (eV)	ϕ_B-ϕ_C (eV)	d (NM)
Cr02	$(2.6\pm0.2)\times10^{9}$	1.68±0.03	-1.6±0.5	1.19±0.05
Cr05	$(6.5\pm0.6)\times10^{8}$	1.87±0.03	0.5±0.5	1.27±0.05
Cr12	$(2.7\pm0.2)\times10^{7}$	1.92±0.05	1.2±0.5	1.54±0.05
Cr05 annealed	$(2.0\pm0.5)\times10^{2}$	2.68±0.02	-2.0±1.0	2.31±0.05
Cr12 annealed	$(2.5\pm0.5)\times10^{2}$	2.66±0.05	-2.5±1.0	2.20±0.05
Cr19	$(2.1\pm0.4)\times10^{-1}$	1.84±0.03	-0.5±0.5	3.51±0.05
Cr19 annealed	$(9.7\pm0.7)\times10^{-3}$	1.88±0.03	-0.5±0.5	3.87±0.05
Cr30	$(3.3\pm0.8)\times10^{7}$	2.10±0.05	3.0±2.0	1.47±0.05

G_0 is the zero-bias specific conductance, $\phi_a = (\phi_B + \phi_C)/2$ the average barrier height, ϕ_B and ϕ_C being the barrier heights at the interfaces with, respectively, the base electrode (Al) and counter-electrode (Nb), and d for $m/m_0 = 0.5$. Notice that the barrier asymmetry data are much less accurate that those for ϕ_a and d, probably indicating substantial deviations of the real barrier profile from the trapezoidal model.

Endurance measurements on the Cr12 wafer were obtained where the relative change in current was monitored at constant applied voltages 0.5V, 0.75V, and 1V. Figure 12 shows the ratio of the electrical current I and the initial current I_0 measured at t=0 s. The various levels of the initial current through the junctions are also indicated. The results for V=1 V show that current changes ~13% after about 1 h of constant stress, which corresponds to ~19X10^6 C/cm^2. It should be mentioned that the junctions were not broken after about one hour of stress.

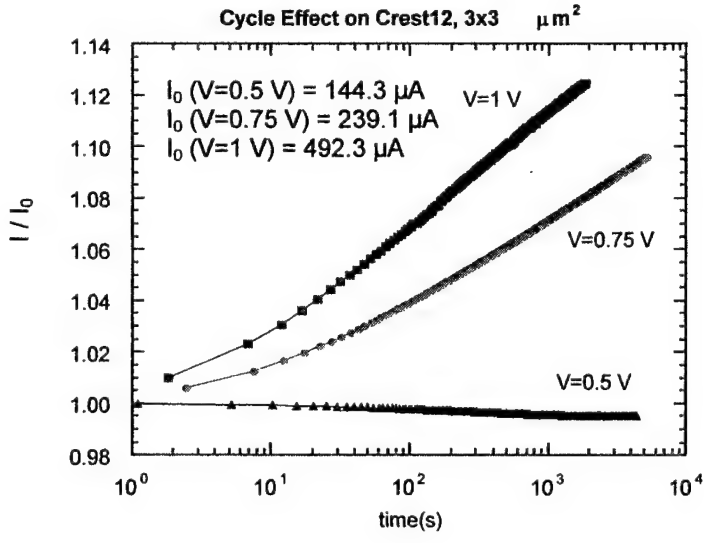

Figure 12. Current ratio I/I(t=0s) as a function of open state time for Cr12 barriers stressed at constant applied voltage.

The endurance performance of Cr 19 barrier junctions was tested under constant applied voltage and constant applied current stress, as well as during voltage cycling with frequency as high as $3x10^4$ cycles/sec.

For instance, on applying a constant current of I=0.7 mA (initial voltage drop of ~ 3V) on a fresh Cr19 junction, we found a time to breakdown (TBD) of 8500 sec, which corresponds to a charge to breakdown of $6.6x10^5$ C/cm^2. Constant voltage stress tests indicated about the same TBD (~10^4 sec) for voltages just below the breakdown value (~3.7) V, with a fast increase for lower voltages.

The effect of cycling frequency on the current-time characteristics of the junctions was also determined. The measurements were performed using voltage pulses of 2.5 V and frequencies spanning over 4 decades. Figure 13a shows the change in the current with respect to the initial value I_0 measured at t = 0 sec as a function of the open state time (time of nonzero applied voltage) for various cycling frequencies. The main result is the almost perfect overlap of the data curves for various frequencies. This suggests that the effect of stress on the current-time behavior is practically independent on voltage cycling, the changes in current being triggered only by the application of the electrical stress. This conclusion is also illustrated in Fig 13b, which shows the same current ratio as a function of the number of cycles, for three open state times, separated by a decade. For a constant open time, the current ratio is independent of the number of cycles.

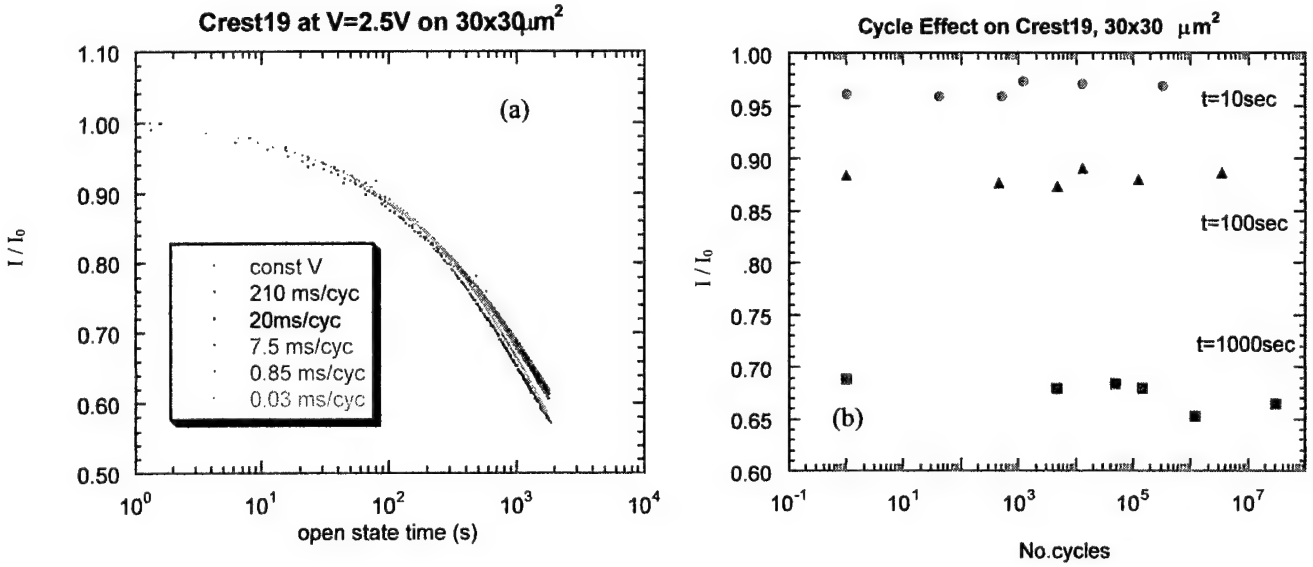

Figure 13. a) Current ratio I/I(t=0s) vs the open state time for V=2.5 V. b) Same current ratio as a function of the number of cycles for a constant open state time t of 10 s, 100 s, and 1000 s.

It is evident that the increase of oxygen exposure leads to a gradual increase of barrier height and thickness, as expected. The results also show high endurance of the barriers at various levels of electrical stress under both constant and cycled applied stress. Unfortunately, however, even the maximum thickness (reached on wafer Cr12) is still too small to be used as one of the crested barrier layers. (Optimally, side layers have to be close to 2.5 nm.) For this reason, high-temperature oxidation and post-annealing of AlO_x barrier structures were explored.

High Temperature Thermal Aluminum Oxide Barriers - According to a recent interesting paper [19], increase of the oxidation temperature leads to the gradual transformation of amorphous aluminum oxide into γ-phase Al_2O_3, but if the temperature is moderate (~ 400°C) and the annealing time is not too high, the structure of ultrathin films may stay very uniform. Unfortunately, the data presented in Ref. 19 are insufficient to determine such crucial parameters of the oxide films as potential barrier height, but since crystalline Al_2O_3 has very broad bandgap (~8.8 eV), and hence the potential barrier height,[2] it was natural to assume that the barrier would grow as oxidation temperature rises.

In order to check this hypothesis, we have fabricated wafer Cr30 with oxide formed at 400 °C, at oxygen pressure of 12mTorr for 6 sec. Figure 14 shows a typical characteristic of the resulting tunnel barrier and its fitting. The results (see also the last row of Table 3) show that the obtained barrier is not specifically thick (probably, due to low oxygen exposure) and (more importantly) not much higher that those of the barriers obtained by low temperature oxidation.

A possible explanation of this fact is that it is more energy advantageous for the oxygen ions, diffusing through the already formed oxide layer, to oxidize new aluminum atoms at the Al/AlO_x interface than to complete the AlO_x structure to the "full" quasi-crystalline Al_2O_3. Though this hypothesis still has to be checked by repeating the experiment as higher oxygen exposures, it implies that annealing of complete samples with a "sealed" amount of oxygen in the oxide layer may be more effective for the barrier height increase.

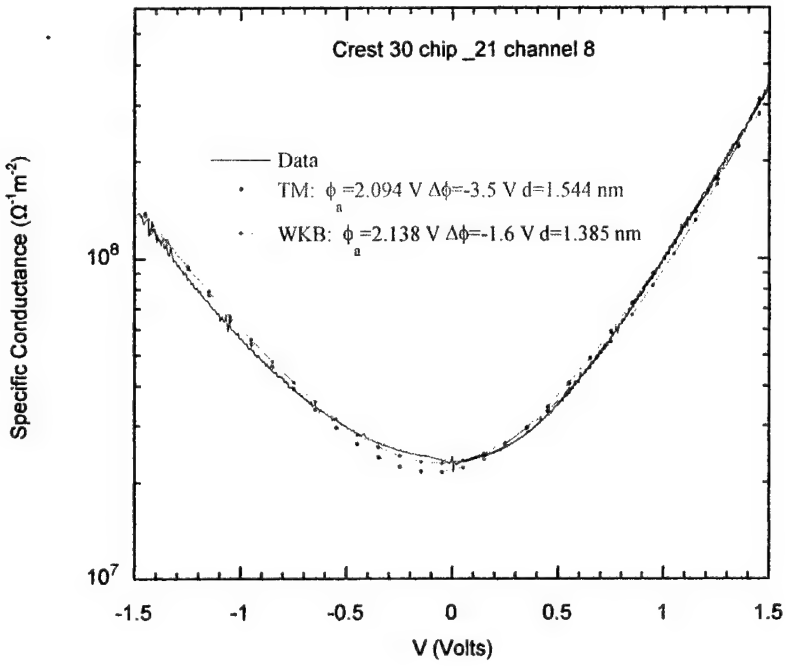

Figure 14. Nonlinear specific conductance of a typical sample from Wafer Cr30.

[2] According to some not very well documented information, up to 3.5 eV.

High Temperature Annealed Aluminum Oxide Barriers - In order to verify this assumption, rapid thermal annealing[3] was employed to treat samples from wafers Cr02, Cr05 and Cr12 for 30 and 60 seconds at 400°C. Figures 15 a and b (as well as blue and green points in Figure 7, and the corresponding rows of Table 3) show typical results of this treatment.

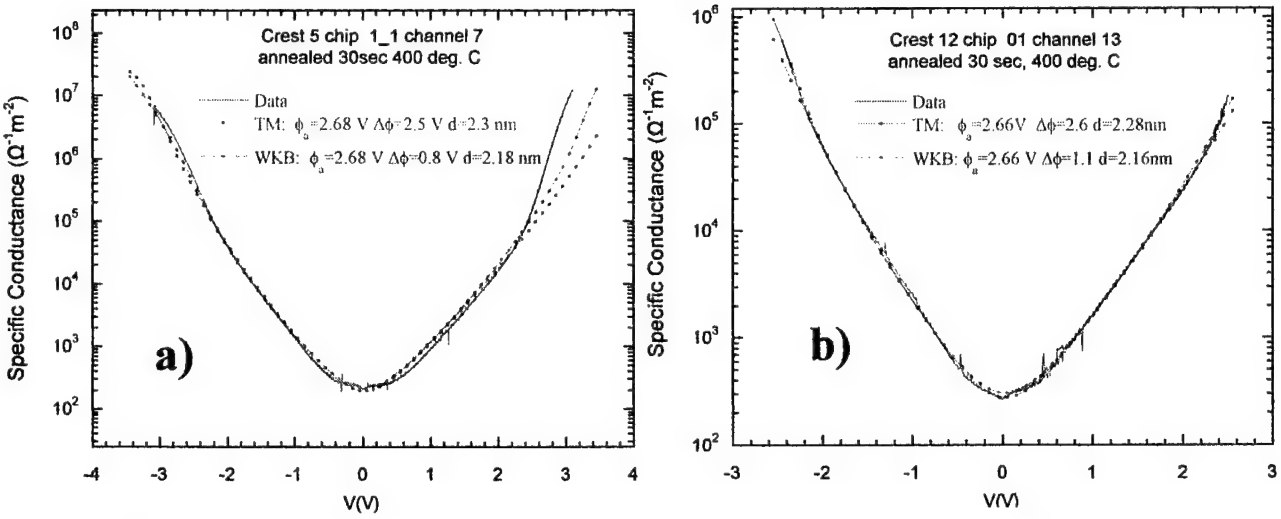

Figure 15. Nonlinear specific conductance of typical annealed samples from wafers a)Cr05 and b)Cr12.

The most evident result of the annealing was a substantial increase of the barrier height, crudely from 1.9 to 2.7 eV (Table 3) and the resulting dramatic (by 6 to 7 orders of magnitude!) increase of the tunnel resistance. Probably less spectacular, but at least equally important, was a significant increase of the breakdown voltage, frequently beyond 3 Volts, corresponding to electric field as high as ~15 MV/cm. On the negative side, the barrier thickness, though increased slightly (to ~ 2.3 nm) is still insufficient for the use of such annealed oxide as the middle layer of the crested barrier. (The desired thickness of this layer is 4 to 6 nm.) The increase of the annealing time from 30 to 60 seconds gave virtually no result.

Plasma Oxidized Barriers - In order to explore various possibilities to increase the aluminum oxide thickness, we have developed a method of barrier oxidation in rf oxygen plasma. Figure 16 (together with Table 3) shows typical results of this procedure, with and without post-annealing. The plasma oxidation for this particular wafer (Cr19) was carried out for 3 minutes at oxygen pressure of 15 mTorr.

One can see, first of all, that the result fitting by microscopic theory of tunneling is not completely satisfactory in this case. Two reasons (and most probably their combination) may be responsible for this fact: 1) the potential barrier profile is substantially different from the employed trapezoidal model, and 2) our theory does not take into account the effect of fast energy relaxation of "hot" (ballistic) electrons in classically-allowed regions of the profile.

The latter effect is important only for layers that are sufficiently thick and robust, that can withstand applied voltages exceeding the barrier height (expressed in eV). In this case naïve tunneling theory (like ours) describes substantial current oscillations due to overbarrier reflection of the ballistic electrons. In reality, energy relaxation suppresses this effect and the oscillations.

[3] The kind help by Dr. X. Wang of Yale University in arranging this procedure is highly appreciated.

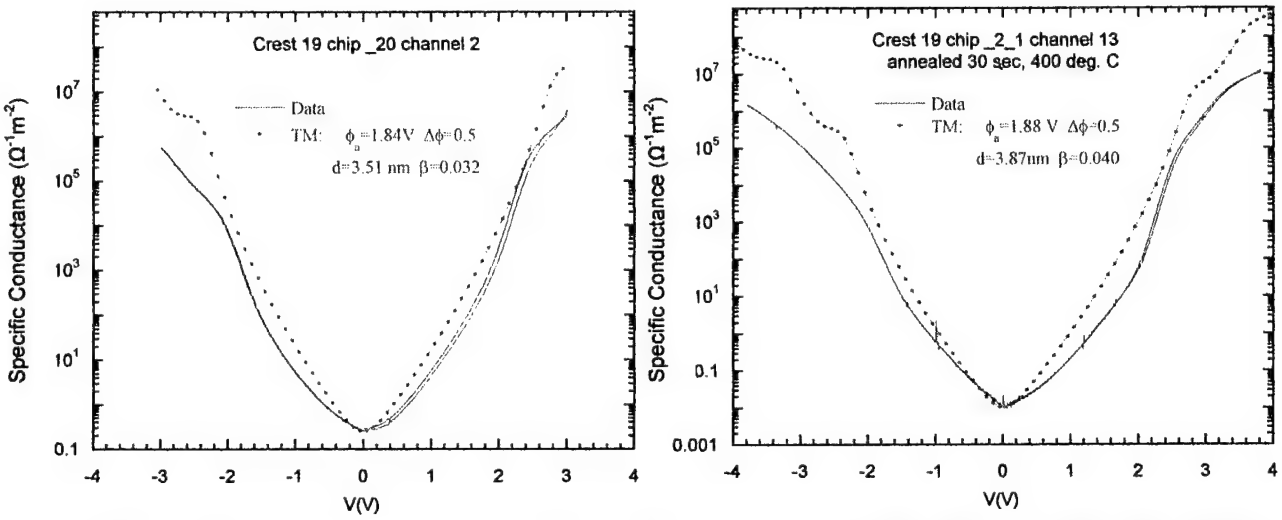

Figure 16. Tunneling characteristics of plasma-oxidized barriers (wafer Cr19) without and with post-annealing.

Work on the improvements of the theoretical program at Stony Brook are in progress, however, even the current fitting capability allows for estimates the barrier parameters (Table 3). The results show that the plasma-oxidized barriers may be rather thick (probably up to 10 nm), but their height is relatively low – close to 1.85 eV. (Post-annealing at 400°C does not change the parameters substantially.)

PLD Aluminum Oxide Barriers at AFR

Figure 17 presents typical *J-V* curves obtained for PLD aluminum oxide barrier layers deposited on p+ silicon at nominal thicknesses of 2, 3 and 4 nm. Deposition parameters were as follows: substrate temperature = 300 °C, laser fluence = 2.0 J/cm^2, repetition rate = 10 Hz, oxygen pressure = 0.05 mTorr. Two important observations are evident from this data: 1) the *J-V* curves are not very dependent of the Al_2O_3 thickness and, 2) the current at negative voltages (electron injection from p^+ Si substrates) is much smaller than at the opposite polarity (electron injection from Al electrode).

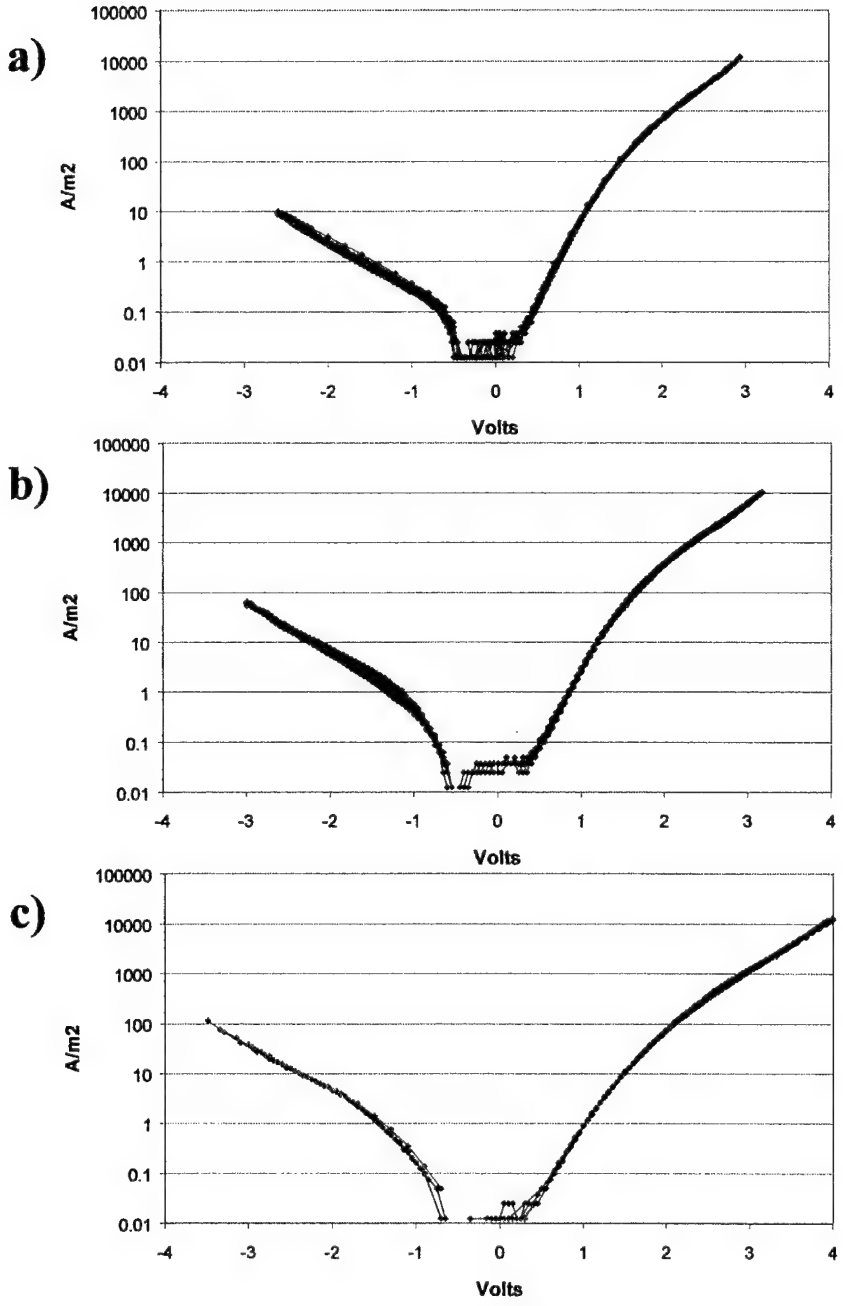

Figure 17. J-V curves for PLD aluminum oxide films grown directly on p+ silicon substrates: a) ~2 nm thick, b) ~ 3 nm thick and c) ~ 4 nm thick. The weak dependence of current on the layer thickness suggests the presence of a thin but high barrier interfacial layer.

Regarding the negative voltages, the current is limited by a *p-n* junction formed in the substrate. The band edge diagrams are depicted in Figure 18.

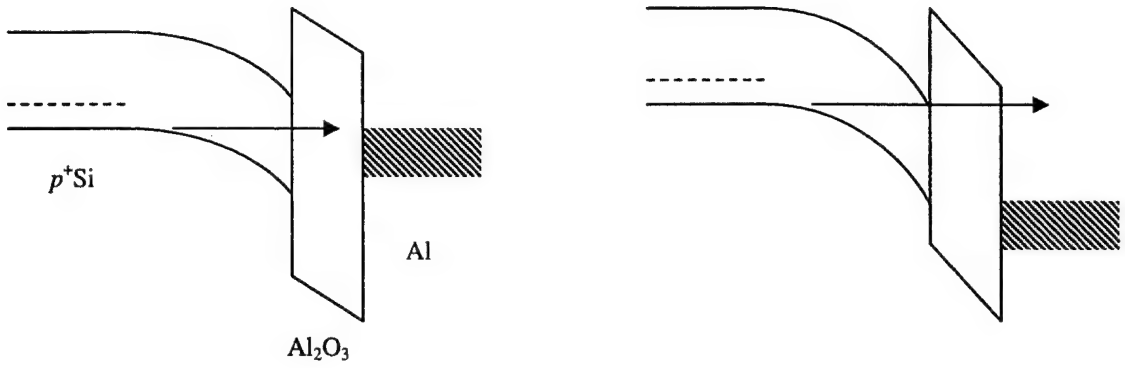

Figure 18. Band edge diagrams for a) small negative voltages ($-V < V_t$) and b) large negative voltages ($-V > V_t$).

Electrons from the valence band of Si do not have available free states in Al until the negative voltage $-V$ exceeds the threshold value V_t at which the Fermi level in Al is aligned with the valence band edge in Si. Assuming that at the flat band voltage the Fermi level of Al divides the silicon bandgap as 1:2 (typical for well conducting metals), we get an estimate Vt ~ 0.7 V, in good accordance with the experimental data. Also, a crude calculation of the Zener current at $-V > V_t$ gives results that agree with experiment for silicon doping ~ 5×10^{19} cm^{-3}, well within the range of the silicon wafer manufacturer's specification.

Regarding the positive voltages, the shape of the log j vs. $-V$ curves is typical for tunneling through a thin and high barrier. Figure 19 shows results of numerical calculation of such current for a bilayer barrier model with the following parameters:

1. Thicker barrier (closer to electron source): thickness = 4 nm, barrier height = 0.4 eV;
2. Thinner barrier (closer to electron drain): thickness = 1.75 nm, barrier height = 4.5 ev.

The curve shown in Figure 19 is reasonably close in magnitude to the experimental results for the PLD barrier layers. This coincidence may imply the presence of a thin, high-barrier layer at the silicon-aluminum oxide interface, possibly the formation of an aluminum silicate interlayer. The calculation also suggests that the barrier height of the PLD layers is lower than barrier heights measured for the post-oxidized aluminum oxide films.

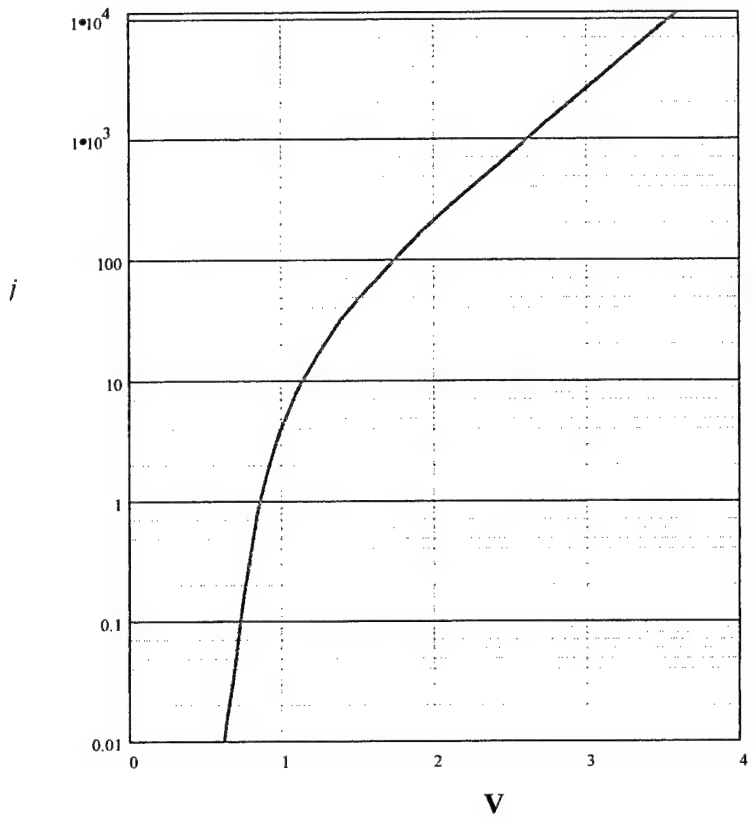

Figure 19. DC *I-V* curve calculated for bilayer barrier with parameters described in the text. Voltage is in Volts, current density in A/m^2.

Other researchers have shown that ultrathin Al_2O_3 films with atomically abrupt interfaces can be grown on silicon, using low energy deposition techniques such as atomic layer deposition (ALD) [20] or thermal evaporation of aluminum with post oxidation [21]. One potential problem that can occur in PLD or other energetic deposition methods such as sputtering or ion beam deposition (IBD) is that of film/substrate atomic mixing [22]. Highly energetic target atoms can penetrate the substrate surface, displacing substrate atoms. Brice et al. [22,23] developed a guide for predicting this ballistic-collision effect, which depends on the substrate mass, the deposited atom mass and energy and the displacement energies. In the case of Al atoms on Si, this atomic mixing can occur at energies as low as 11 eV. Note that techniques such as ALD and thermal evaporation have energies in the 0.1 eV range.

A straightforward way to deal with this potential problem of silicate formation is to deposit a relatively thick aluminum base electrode layer on the silicon substrate and then build the aluminum oxide layers on this foundation. During this Phase I, AFR attempted to deposit PLD layers on Al-coated silicon, however, the junctions typically exhibited electrical shorts. One explanation is that the deposited aluminum oxide films are non-uniform, possibly due to poor wetting resulting in island growth and non-continuous coverage of the Al layer. On the other hand, atomic mixing may also be a problem for the PLD films deposited on Al, using the deposition parameters established during this Phase I project. More work is needed to explore the effects of the PLD deposition parameters, mainly the laser fluence and background gas (reactive and/or inert) which strongly affect the energies of the plume species.

The apparent interlayer (inferred through the *I-V* data) observed in the PLD barrier structures prevented an accurate determination of the PLD aluminum oxide barrier height. However, the *I-V* measurements did allow us to reasonably estimate the breakdown strength of the PLD aluminum oxide. Table 4 lists soft breakdown voltages measured for several samples at varying thicknesses (estimated based on deposition rate) ranging from 2.0 – 4.4 nm.

Table 4. Breakdown voltages measured for several PLD aluminum oxide barriers

Sample Name	Estimated Barrier Thickness (nm)*	No. Junctions Measured to Breakdown	Average Soft Breakdown Voltage (V)	Soft Breakdown Voltage Range (V)
F020706a	2.0	4	2.5	2.0 – 2.8
F020630b	3.0	4	3.18	3.0 – 3.32
F020704a	4.0	6	3.85	3.5 – 4.15
F020706b	4.0	3	4.15	4.05 – 4.2
F021009a	4.4	3	4.32	4.0 – 4.5

* based on the PLD deposition rate

The thicknesses listed in Table 4 do not account for the thin, high barrier interlayer we believe is present in these PLD aluminum oxide films deposited on bare silicon. If we assume that the interlayer adds ~ 1.0 nm to the thickness of each sample (based on the above calculation, assuming that the interlayer thickness is similar for each film), then the breakdown field is > 7.5 MV/cm for the PLD oxide layers.

Task 3 – Manufacturing Studies

Objective: To evaluate deposition technologies for fabricating crested tunnel barriers.

Work Performed: Phase I examined three possible deposition technologies to be investigated in Phase II: atomic layer deposition (ALD), biased target ion beam deposition (BTIBD) and sputter deposition.

ALD is a special type of CVD that involves a sequence of pulsed precursor gases and inert sweep gases, rather than the mixing of gases employed in traditional CVD. Through "chemisorption", a monolayer of precursor gas is absorbed onto the wafer surface. Any excess gas is removed and a reactant gas is introduced, which reacts with the first layer to form the desired film. ALD is an inherently self-limiting and layer-by-layer deposition process, i.e., it produces very thin films with excellent uniformity. High quality aluminum oxide films have been demonstrated by others [20]. ALD reactors are amenable to batch-processing and are also relatively simple in design, where the gas handling equipment represents the most complex component(s) of the reactor.

BTIBD utilizes principles of ion beam deposition (IBD) and ion-assisted deposition (IAD). BTIBD is attractive for several reasons including, 1) excellent deposition rate control (down to 0.1 Å/sec), 2) ability to deposit a wide variety of materials, from metals to dielectrics, 3) excellent control of adatom energy, independent of deposition rate, potentially providing improved film properties (microstructure, density, etc.), and 4) through "electronic shuttering", a fast on-off deposition environment can be achieved.

Traditional magnetron sputtering (DC or RF) is also an attractive deposition technology for depositing aluminum oxide tunnel barrier layers. The process can be highly energetic (although the potential for atomic mixing exists if the energies of sputtered atoms are too high), allows for low deposition rates if needed and provides an on-off deposition environment through electronic

or mechanical shuttering. Oxides such as Al_2O_3 can be deposited using an Al_2O_3 target (RF mode) or by reactive sputtering of a pure aluminum target in an Ar/O_2 background, which can be considered as an "in-situ plasma oxidation". Perhaps even more importantly, however, were the successes achieved at Stony Brook with post-oxidized sputter deposited Al layers during Phase I. We therefore intend to focus on sputter deposition (post-oxidized Al and deposited Al_2O_3) during Phase II.

Under a Small Business Innovative Research (SBIR) Phase II project supported by the National Science Foundation (NSF), AFR modified a rapid thermal processing (RTP) chamber for reactive dc magnetron sputter deposition. The high vacuum RTP system, shown in Figure 20, incorporates a six-zone,10 kW linear quartz lamp heater and wafer rotation for processing 150 mm wafers up to 1000 °C. A two-inch magnetron sputtering source (AJA International model ST20) was installed for deposition of metallic and dielectric thin film materials. As shown, the sputter source includes a gas ring and chimney for delivery of the argon sputter gas. For reactive oxide deposition, oxygen is introduced near the substrate surface. The intent of this arrangement is to maintain a relatively high partial pressure of oxygen at the substrate and a lower partial pressure of oxygen at the sputter target, to minimize "poisoning" (oxidation) of conductive targets (metals or doped semiconductors). The chimney also restricts the line-of-sight of the source to only the substrate, thus minimizing material deposition on chamber walls and viewports, etc. While the emphasis of the NSF program is to develop a whole wafer sensor for real-time monitoring during thermal processing of semiconductor-related materials, the facility was used to demonstrate feasibility of depositing Al_2O_3 by reactive DC magnetron sputtering for this Phase I program.

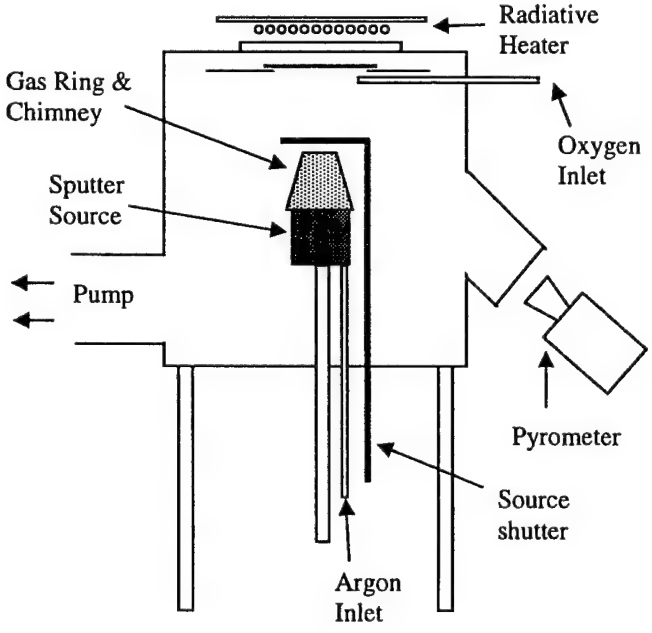

Figure 20. RTP system at AFR showing single two-inch magnetron sputter source.

Figure 21 displays an infrared reflectance spectrum measured for an ~ 72 nm thick aluminum oxide film grown on silicon using the reactive sputter system. Deposition parameters were: pressure = 2.4 mTorr, Ar flow rate ~ 5 sccm, O_2 flow rate ~ 2 sccm, substrate temperature ~ 300 °C, gun power = 100 W. Similar to the PLD IR film measurement shown in Figure 4, the spectrum exhibits a sharp absorption feature characteristic of Al_2O_3. An

RBS measurement shown in Figure 22 confirms the stoichiometeric Al/0 relationship (0.4/0.6) in the film. The deposition rate for this set of conditions was ~ 0.1 nm/sec, which is suffieciently low pfor production of ultrathin films in the 2 – 6 nm range.

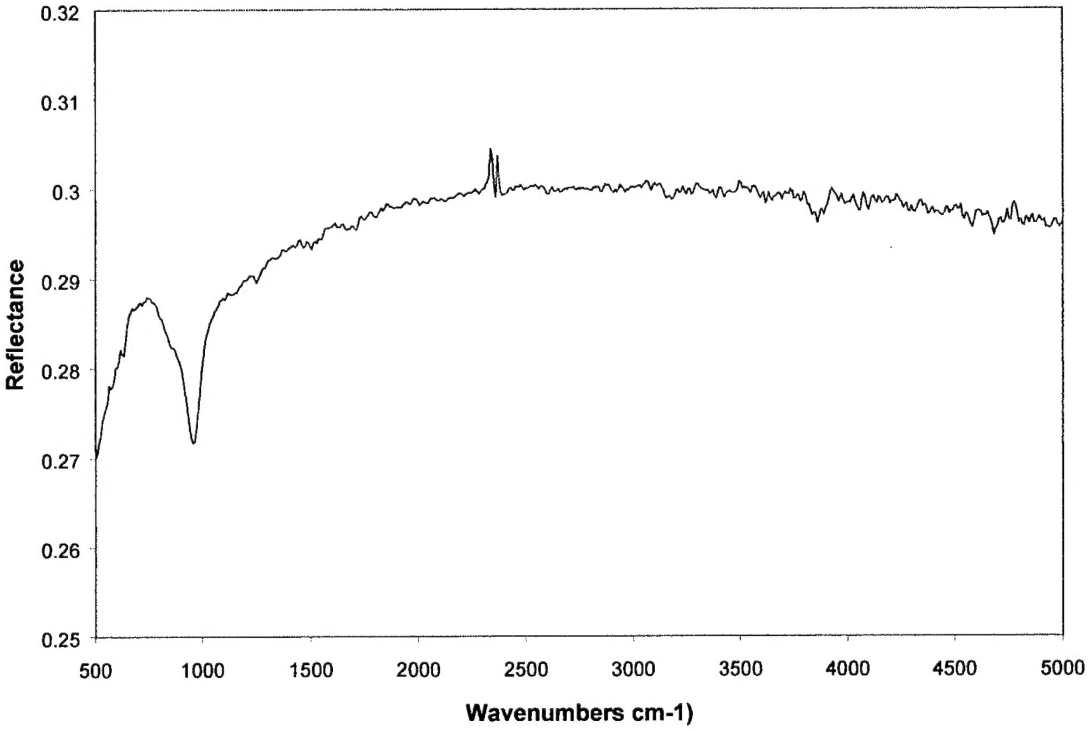

Figure 21. Infrared reflectance spectrum measured for an aluminum oxide film deposited by reactive DC magnetron sputtering

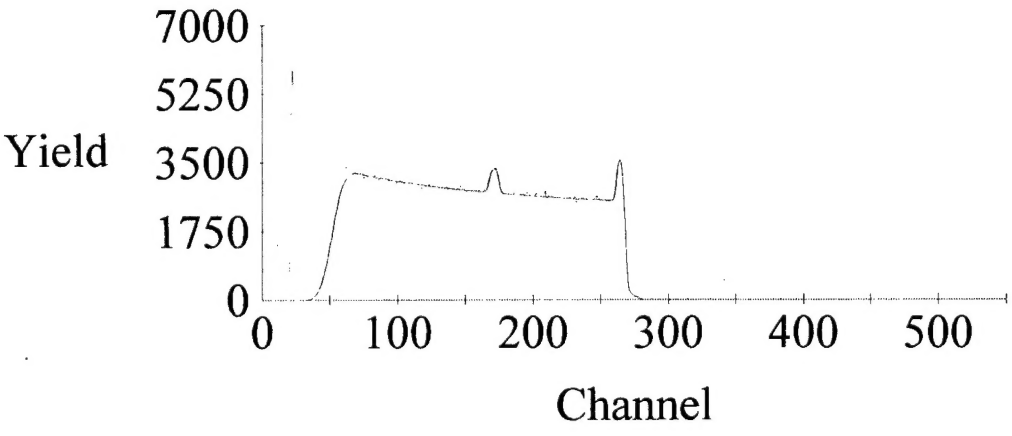

Figure 22. RBS measurement of an aluminum oxide film deposited by reactive DC magnetron sputtering. The measurement confirms stoichiometric Al/O relationship.

d. Conclusions

The experimental results in this Phase I program clearly show technical feasibility, successfully demonstrating the following.

- The post-oxidized aluminum oxide tunnel barriers fabricated at Stony Brook showed high breakdown fields, ≥ 10 MV/cm, and exhibited excellent endurance under high electric stress.
- The post-oxidized tunnel barrier characteristics (barrier height) could be altered by varying methods and parameters of oxidation, without a breach of high uniformity of the barriers.
- AFR demonstrated the ability to deposit stoichiometric Al_2O_3 by the methods of pulsed laser deposition (PLD) of alumina and reactive DC magnetron sputtering of a pure aluminum target in a background gas of oxygen and argon.
- Although the barrier characteristics of the PLD aluminum oxide films grown on silicon at AFR could not be accurately determined (due to the likely formation of a thin interlayer), the films as thick as 4.4 nm exhibited high breakdown fields conservatively estimated at > 7.5 MV/cm.

Based on these results, continuation onto Phase II is clearly called for, where the research will focus on combining various aluminum oxide layers with each other, and possibly with other high-performance materials like SiO_2, to form good crested barriers. Preliminary computer modeling of the crested barriers using already developed Al_2O_3 layers shows that combinations of the plasma-oxidized AlO_x layer, similar to that on wafer Cr19, with either the annealed layer similar to Cr12, or with 4-nm of SiO_2, should already give barrier performance (steepness of the $\log j$ – vs.-V curve) substantially better than the currently used uniform, silicon dioxide barriers (Figure 23). In addition, there is little doubt that further adjustment of the barriers, for example, the increase of Cr12 thickness (that apparently may be achieved by oxidation at higher temperature plus additional annealing) may lead to considerably better results.

Phase II research will have two major thrusts:

1) Continued development and optimization of both post-oxidized aluminum oxide tunnel barriers and deposited aluminum oxide barriers (sputtering, PLD) and,
2) Fabrication of bilayer tunnel barrier devices.

Areas in need of further investigation include:

- Effects of higher oxygen exposure and temperature and post-annealing on both thermal aluminum oxide layers and plasma-grown aluminum oxide.
- Effects of critical process parameters involved in deposited aluminum oxide layers using sputtering (temperature, pressure, gun power) or PLD (temperature, pressure, laser fluence) as well as the effects of rapid thermal post-annealing.
- Methods of combining low and high barrier oxide layers. A likely scenario would be to start with a plasma-grown oxide, followed by deposition a thin Al layer with thermal oxidation and post-annealing. Alternatively, the second layer could be a sputter or PLD grown oxide.
- Existing theoretical codes for tunnel modeling should be further improved to include the following effects:
  - more complex barrier profiles,
  - inelastic relaxation of hot electrons, and
  - effects of accumulation of electric charge of tunneling electrons.

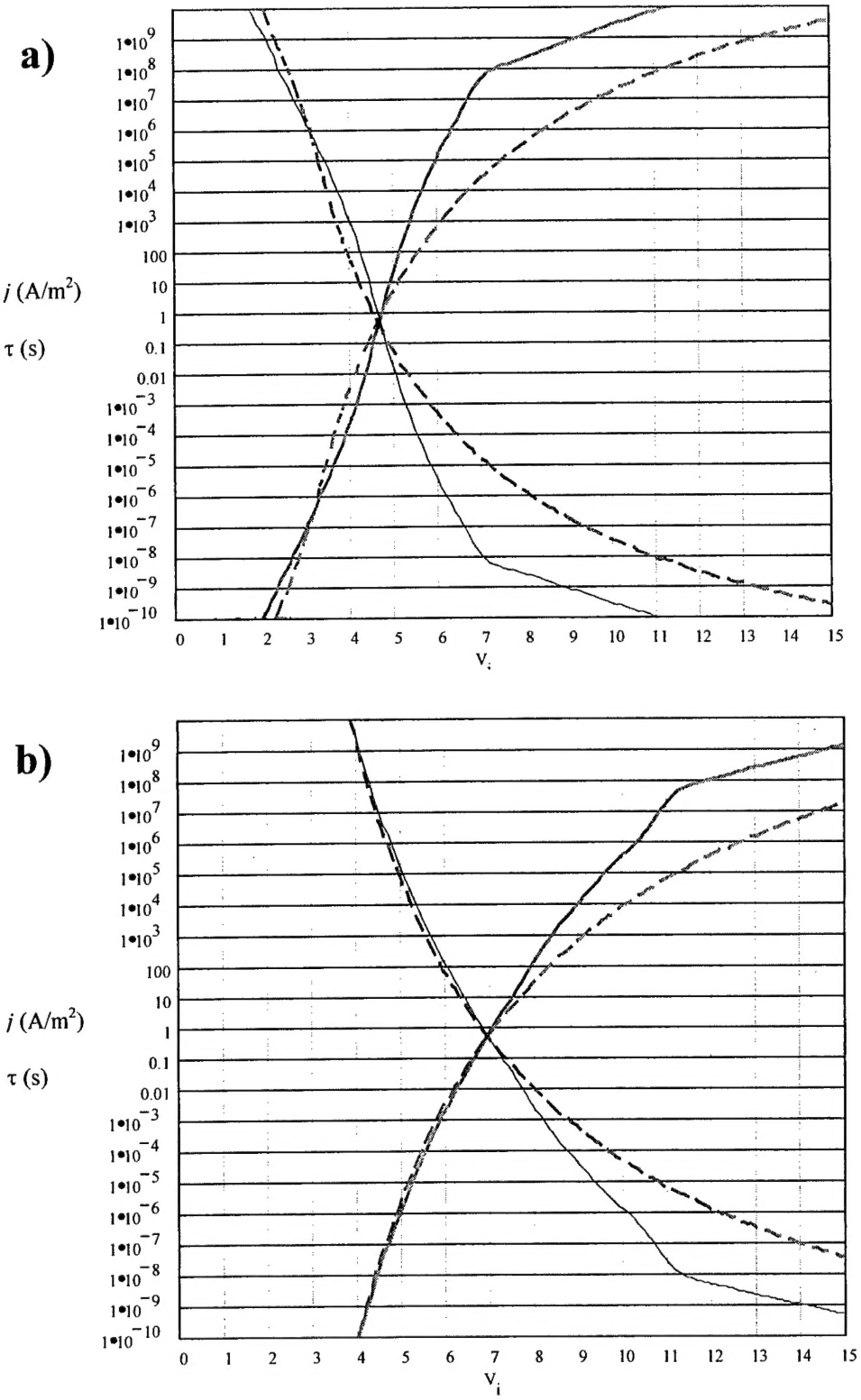

Figure 23. Theoretical (WKB) results for current (red lines, in A/m^2) and floating gate recharging time scale (blue lines, in seconds) as functions of voltage (in Volts) for the following trilayer barriers: a) Cr19/Cr12annealed/Cr19 and Cr19/4-nm-SiO_2/Cr19. Dashed lines show the corresponding results for uniform SiO_2 barriers of comparable thickness: 7nm in (a) and 9 nm in (b).

References

1. A. K. Sharma, *Semiconductor Memories* (IEEE Press, New York, 1997).
2. *Nonvolatile Semiconductor Memory Technology*, ed. by W. D. Brown and J. E. Brewer (IEEE Press, New York, 1998).
3. K. K. Likharev, "Layered tunnel barriers for nonvolatile memory devices," *Appl. Phys. Lett.*, vol. 73, pp. 2137-2139, Oct. 1998.
4. A. N. Korotkov and K. K. Likharev, "Resonant Fowler-Nordheim tunneling and its possible applications", in: *1999 IEDM Tech. Digest* (IEEE Press, Piscataway, NY, 1999), pp. 223-226.
5. K.K. Likharev, "Riding the Crest of a New Wave in Memory," *Circuits & Devices*, p. 16, July 2000).
6. D. Y. Zinoviev and Yu. A. Polyakov, "Octopux: An advanced automated setup for testing superconductor circuits", *IEEE Trans. Appl. Supercond.*, vol. 7, pp. 3240-3243, June 1997.
7. Hubler, G.K., "Comparison of Vacuum Deposition Techniques," Pulsed Laser Deposition of Thin Films, (edited by D.B Chrisey and G.K. Hubler), p.345 (1994).
8. Hubler, G.K., "Comparison of Vacuum Deposition Techniques," Pulsed Laser Deposition of Thin Films, (edited by D.B Chrisey and G.K. Hubler), p.340 (1994).
9. K. H. Gundlach and J. Höltz, "Logarithmic conductivity of Al-Al_2O_3-Al tunneling junctions produced by plasma- and thermal oxidation", *Surf. Sci.*, vol. 27, pp. 125-141, 1971.
10. D. Meyerhofer and S. A. Ochs, "Current flow in very thin films of Al_2O_3 and BeO", *J. Appl. Phys.*, vol. 34, pp. 2535-2543, Sep. 1963.
11. S. R. Pollack and C. E. Morris, "Electron tunneling through asymmetric films of thermally grown Al_2O_3", *J. Appl. Phys.*, vol. 35, pp. 1503-1512, May 1963.
12. D. McBride, G. Rochlin, and P. Hansma, "Characterization of metal-oxide tunnel-junction barriers", *J. Appl. Phys.*, vol. 45, pp. 2305-2312, May 1974.
13. K. Gloss, P. J. Koppinen, and J. P. Pekola, "Properties of native ultrathin aluminum oxide tunnel barriers", preprint, July 2002.
14. J. G. Simmons, "Low-voltage current-voltage relationship of tunnel junctions", *J. Appl. Phys.*, vol. 34, pp. 238, Jan. 1963; "Generalized formula for electric tunnel effect between similar electrodes separated by thin insulating film", *J. Appl. Phys.*, vol. 34, pp. 1793, June 1963; "Electric current effect between dissimilar electrodes separated by a thin insulating film", *J. Appl. Phys.*, vol. 34, pp. 2581, Sep. 1963.
15. W. F. Brinkman, R. C. Dynes, and J. M. Rowell, "Tunneling Conductance of Asymmetrical Barriers", *J. Appl. Phys.*, vol. 41, pp. 1915, May 1970.
16. R. E. Miller, W. H. Mallison, A. W. Kleinsasser, K. A. Delin, and E. M. Macedo, "Niobium trilayer Josephson tunnel junctions with ultrahigh critical-current densities", *Appl. Phys. Lett.*, vol. 63, pp. 1423-1425, Sep. 1993.
17. K. K. Likharev, "NOVORAM: A New Concept for Fast, Bit-Addressable Nonvolatile Memory Based on Crested Barriers". *IEEE Circuits and Device*s, vol. 16, pp. 16-21, Apr. 2000.
18. N. W. Ashcroft and N. D. Mermin, *Solid State Physics*. Fort Worth, TX: Saunders, 1976, p.38
19. P. C. Snijders, L. P. H. Jeurgens, and W. G. Sloof, "Structure of thin aluminum-oxide films determined from valence band spectra measured using XPS", *Surface Science*, vol. 496, pp. 97-109, Jan. 2002.
20. Gusev, E.P., Copel, M., Cartier, E., Baumvol, I.J.R., Krug, C., and Gribelyuk, M.A., *Appl. Phys. Lett.*,vol. 76 pp. 176-178 (2000).
21. Kundu, M., Miyata, N. and Ichikawa, M., *Appl. Phys. Lett.*, vol. 78, pp. 1517-1519 (2001).
22. Hubler, G.K., "Comparison of Vacuum Deposition Techniques," Pulsed Laser Deposition of Thin Films, (edited by D.B Chrisey and G.K. Hubler), p.335 (1994).
23. Brice, D.K., Tsao, J.Y. and Picraux, *Nucl. Instrum. Meth. Phys. Res.*, B44, p. 68 (1989).